Self-assembly and intra-cluster reactions of erbium and ytterbium bis(2-ethylhexyl)sulfosuccinates in the gas phase

Serena Indelicato[1,2], David Bongiorno[1,2]*, Vincenzo Turco Liveri[1], Andrea Mele[3], Walter Panzeri[4], Francesca Castiglione[3] and Leopoldo Ceraulo[1,2]

[1]Department STEBICEF, University of Palermo, Via Archirafi n.32, I-90123, Palermo, Italy
[2]CGA-UniNetLab, University of Palermo, Via F. Marini n.14, I-90128, Palermo, Italy
[3]Department of Chemistry, Materials and Chemical Engineering "G. Natta" Politecnico di Milano, Via L. Mancinelli n. 7, I-20133, Milano, Italy
[4]CNR-Istituto di Chimica del Riconoscimento Molecolare, Via L. Mancinelli n.7, I-20133, Milano, Italy

Surfactant self-assembling in the gas phase, leading to the formation of structurally organized supramolecular aggregates, is a topic of considerable interest.[1] From a theoretical point of view, the study of micellar systems in the gas phase is expected to add fundamental knowledge on anisotropic surfactant–surfactant interactions in the absence of solvent molecules and their chemical and physical properties while novel applications of surfactant assemblies in the gas phase include possible drug and intact protein carriers, air-cleaning agents and exotic nanoreactors for specialized chemistry. As biomembrane models, micelles are used to gather information on processes of partitioning and localization of vitamins, hormones and other co-factors, and to study their role and biological activity.[2–5]

The occurrence of micellar aggregates in the gas phase was demonstrated by electrospray ionization mass spectrometry (ESI-MS) in the milestone paper of Siuzdak and Bothner.[6]

* *Correspondence to:* D. Bongiorno, Department STEBICEF, University of Palermo, Via Archirafi n.32, I-90123 Palermo, Italy.
E-mail: david.bongiorno@unipa.it

More recently, several research groups have focused on their structural characterization and their ability to incorporate solubilized molecules.[7–22]

We have extensively studied the self-assembling of sodium bis(2-ethylhexyl)sulfosuccinate (AOTNa), one of the most popular surfactants yielding reverse micelles in apolar solvents, by ESI-MS, energy-resolved mass spectrometry (ER-MS), infrared multiphoton decomposition (IRMPD), ion mobility mass spectrometry and molecular dynamics simulations.[11–20] The experimental and theoretical findings concurred to suggest an aggregate structure characterized by a charged hydrophilic core formed by surfactant head groups and sodium counterions surrounded by an apolar shell constituted by the surfactant alkyl chains. As a consequence of strong coulombic interactions, charged heads and counterions form a solid-like core at which the AOTNa alkyl chains, that show relatively high mobility, are anchored. The pivotal role of the electrostatic forces in the AOTNa self-assembling in the gas phase has also been emphasized by the marked effects on the stability and relative abundance of the aggregates caused by the substitution of the sodium counterion with other alkali metal ions,[23] or divalent cations.[24,25]

Taking into account that the substitution of the counterion of the AOT^- anion (see Fig. 1) with trivalent cations should further amplify these effects and provide the resulting supramolecular aggregates with selected properties dictated by the metal cation (e.g. luminescence and photoactivated metal-ligand electron transfer), we decided to extend our investigations to some lanthanide-functionalized AOTNa derivatives.[26–28]

Here we present a study of the charged aggregates resulting from the electrospray ionization both in positive and negative ion mode of solutions containing $(AOT)_3Yb$ and $(AOT)_3Er$ by ESI-MS, ESI-MS/MS and ER-MS. We will show that, in addition to effects in the organization, abundance and stability of aggregates due to the presence of lanthanide ions, some collision-induced concerted intra-aggregate chemical transformations are observed.

EXPERIMENTAL

Synthesis of surfactant–lanthanide complexes

Sodium bis(2-ethylhexyl)sulfosuccinate (AOTNa, 99%; Sigma-Aldrich, St. Louis, MO, USA) was vacuum-dried for several days. Ytterbium(III) nitrate (Sigma-Aldrich, 99.9%), erbium(III) nitrate (Sigma-Aldrich, 99.9%), acetonitrile, methanol and water (Sigma-Aldrich, LC/MS grade) were used as received. $(AOT)_3Yb$ and $(AOT)_3Er$ were prepared by mixing appropriate amounts of an aqueous solution of $Yb(NO_3)_3$ or $Er(NO_3)_3$ with a 10^{-2} M aqueous solution of AOTNa. The precipitate was filtered, washed with water several times and vacuum-dried at room temperature.

ESI-MS and ESI-MS/MS

Electrospray ionization experiments both in positive and in negative ion mode of $(AOT)_3Yb$ and $(AOT)_3Er$ were performed on a quadrupole-time-of-flight high-resolution LC/MS system (q-Tof Premier; Waters, Milford, MA, USA) under the following conditions: infusion at 5 μL min^{-1} flow rate, sample concentration 0.5 mM (in CH_3CN), capillary voltage 3.0 kV, cone voltage 170 V and 35 V, extraction cone voltage 4.4 V, ion guide voltage 1.2 V, source temperature 90 °C, desolvation temperature 250 °C, desolvation gas (N_2) flow rate 530 L h^{-1}, cone gas (N_2) flow rate 50 L h^{-1}, radiofrequency (RF) settings: autoprofile, mass range: *m/z* 50–8000. For MS spectra (in positive and negative ion mode) a scan time of 1 s and an interscan time of 0.1 s were set. The mass accuracy was ±0.3 Th.

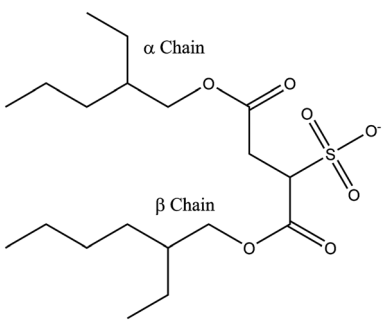

Figure 1. Structure of the bis(2-ethylhexyl)sulfosuccinate anion (AOT^-).

ESI-MS/MS measurements were carried out under the following experimental conditions using a quadrupole-time-of-flight high-resolution LC/MS system (Waters q-Tof Premier): direct infusion at 5 μL min^{-1} flow rate, sample concentration 0.5 mM (in CH_3CN), needle voltage 3.5 kV, sampling cone voltage 170 V, extraction cone voltage 4.4 V, ion guide voltage 1.2 V, source temperature 90 °C, desolvation temperature 250 °C, desolvation gas (N_2) flow rate 530 L h^{-1}, cone gas (N_2) flow rate 50 L h^{-1}, target gas (Ar) pressure $4.5 \cdot 10^{-3}$ mbar, scan time 1 s. In order to obtain an abundance of the precursor ion equal to the 50% of the total ion current, the collision energy (CE) values were optimized.

The Survival Yield (SY) curves for each precursor ion were obtained using the same experimental conditions used for tandem mass experiments, except for the CE values, that were varied by discrete amounts in the range 5–90 eV during the flow injection experiments. For each collision energy an acquisition time of 0.5 min was set and each ESI-MS/MS spectrum was obtained from the average of 11 consecutive scans.

The percentage of each product ion was calculated by dividing the counts of the corresponding peak by the sum of the counts of all the peaks including the precursor ion.

Experimental conditions were maintained constant through the complete set of measurements and each SY curve acquisition of positively and negatively singly charged aggregate ions was repeated three times.

High-resolution MS/MS spectra were obtained using a hybrid quadrupole/orbitrap mass spectrometer (Q-Exactive; Thermo Fisher Scientific, Waltham, MA, USA). All the instrument parameters were controlled by Xcalibur software (Thermo Fisher Scientific) and the ESI-MS/MS spectra were recorded at 140 000 resolving power and using the following experimental setup: spray voltage 3.5 kV, capillary temperature 275 °C, sheath gas (N_2) flow rate 4 arbitrary units, S-lens RF-level 0.

RESULTS AND DISCUSSION

Positive ion polarity: ESI-MS spectra of $(AOT)_3Yb$ and $(AOT)_3Er$

Preliminary experiments were carried out to find the best experimental conditions. Solutions of $(AOT)_3Yb$ and $(AOT)_3Er$ in three different solvents (CH_3CN, CH_3OH and CH_3OH/H_2O 50/50 v/v) were examined. While no significant solvent effect was observed on the aggregate composition and charge state, the best results in terms of signal stability, sensitivity and spectrum reproducibility were obtained using CH_3CN for both positive and negative polarity.

ESI-MS spectra obtained from CH_3CN solutions of $(AOT)_3Yb$ and $(AOT)_3Er$ were recorded at cone voltages of 35 V and 170 V. The results are summarized in (Fig. 2) for $(AOT)_3Yb$ and in Supplementary Fig. S1 (Supporting Information) for $(AOT)_3Er$. The spectra of both surfactants show a collection of peaks consistent with clusters of AOT^- and lanthanides (Ln, Ln = Yb, Er) due to $[(AOT)_{3m-1} + mLn]^+$ species (with $1 \le m \le 5$), and peaks due to $([(AOT)_n + mLn + pNa]^+$ species (with $3 \le n \le 16$; $1 \le m \le 5$ and $1 \le p < 5$) characterized by the

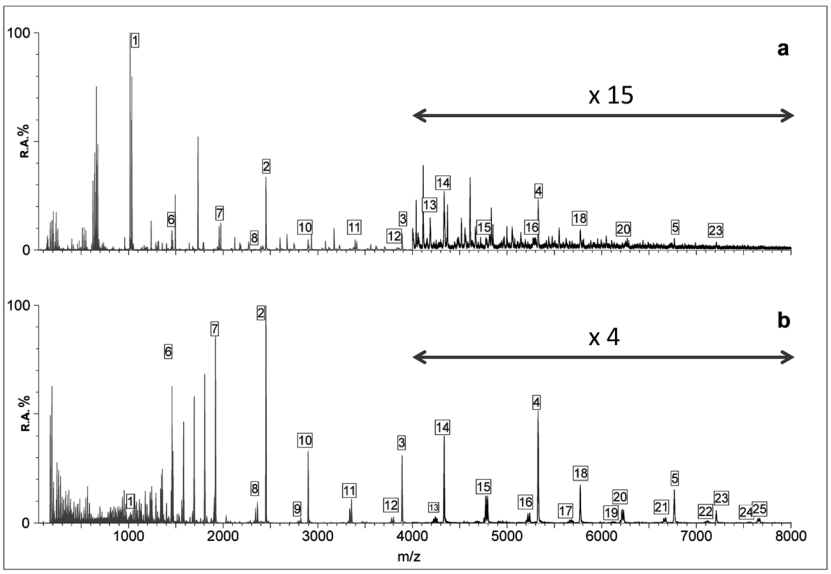

	Species
1	$[AOT_2Yb]^+$
2	$[AOT_5Yb_2]^+$
3	$[AOT_8Yb_3]^+$
4	$[AOT_{11}Yb_4]^+$
5	$[AOT_{14}Yb_5]^+$
6	$[AOT_3YbNa]^+$
7	$[AOT_4YbNa_2]^+$
8	$[AOT_5YbNa_3]^+$
9	$[AOT_6YbNa_4]^+$
10	$[AOT_6Yb_2Na]^+$
11	$[AOT_7Yb_2Na_2]^+$
12	$[AOT_8Yb_2Na_3]^+$
13	$[AOT_9Yb_2Na_4]^+$
14	$[AOT_9Yb_3Na]^+$
15	$[AOT_{10}Yb_3Na_2]^+$
16	$[AOT_{11}Yb_3Na_3]^+$
17	$[AOT_{12}Yb_3Na_4]^+$
18	$[AOT_{12}Yb_4Na]^+$
19	$[AOT_{13}Yb_3Na_5]^+$
20	$[AOT_{13}Yb_4Na_2]^+$
21	$[AOT_{14}Yb_4Na_3]^+$
22	$[AOT_{15}Yb_4Na_4]^+$
23	$[AOT_{15}Yb_5Na]^+$
24	$[AOT_{16}Yb_4Na_5]^+$
25	$[AOT_{16}Yb_5Na_2]^+$

Figure 2. ESI-MS spectra of $(AOT)_3Yb$ at cone voltage values of (a) 35 V and (b) 170 V. The number on each peak indicates the species listed in the right side of the figure.

participation of environmental Na^+ ions. The base peak is that due to the $[AOT_3LnNa]^+$ species, both at 35 V and 170 V. On the other hand, some peaks, due to in-source fragmentation of surfactant aggregates, mainly involving C_8H_{16} (112 Da) elimination, are observed at 170 V while they are absent at 35 V. Moreover, spectra recorded at a cone voltage of 35 V show additional peaks due to some doubly charged aggregates.

No solvated species are observed, suggesting that the counterion/surfactant head interactions are stronger than the counterion/solvent and surfactant head/solvent ones. In this respect, they behave as AOTNa aggregates[10] rather than those of AOT^- with some divalent ions.[24] It is worth noting that the similar ESI-MS behavior of $(AOT)_3Yb$ and $(AOT)_3Er$ reflects the similarity of the chemical properties of the lanthanides.

Positive ion polarity: ESI-MS/MS experiments on AOT Yb and Er aggregates

The structure, stability and fragmentation patterns of AOT-Ln and AOT-Ln-Na aggregates (Ln = Yb, Er) were studied by collision-induced dissociation (CID) experiments. As representative species of AOT-Ln, we studied $[AOT_5Ln_2]^+$ and $[AOT_8Ln_3]^+$ whereas, to illustrate the AOT-mixed metal aggregates, $[AOT_3LnNa]^+$, $[AOT_4LnNa_2]^+$, and $[AOT_6Ln_2Na]^+$ species were investigated.

In order to establish the fragmentation behavior of AOT-Ln aggregates, several MS/MS experiments were performed at various collision energy values (ER-MS). This approach allows us to observe the evolution of the fragmentation pathways from the lowest to the highest value of CE.

Sodium free aggregates: $[AOT_5Ln_2]^+$ and $[AOT_8Ln_3]^+$

The CID experiments of $[AOT_5Yb_2]^+$ were performed by selecting the ion at *m/z* 2447 as the precursor ion, that is the most abundant isotopic species of this cluster. At the lowest collision energy (laboratory frame energy 15 eV), the spectrum shows only a peak at *m/z* 1913, that remains the only product ion observed up to 25 eV (Supplementary Fig. S2, Supporting Information), and whose formation involves the neutral loss of a 534 Da species. The loss of such neutral species, never reported previously for either AOT–alkali metal or AOT–divalent metal aggregates,[10–12,15,23–25] prompted us to investigate the underlying chemistry.

In order to achieve information on its elemental composition, the CID spectrum of the $[AOT_5Yb_2]^+$ ion (*m/z* 2447.00) was also recorded on a Q-Exactive instrument that has a better mass accuracy and a more effective and narrower selection of the precursor ion than the Q-ToF. The accurate mass measurement evidenced a loss of a neutral fragment of 534.35894 Da, that agrees with the formula $C_{28}H_{54}O_7S$ (calculated mass 534.35902). The lack of any peak between the precursor ion (*m/z* 2447) and the product ion (*m/z* 1913) suggests that the elimination of $C_{28}H_{54}O_7S$ occurs in one step. This implies the intriguing fragmentation mechanism described in Scheme 1, which involves a collision-induced intra-cluster nucleophilic attack of the SO_3^- of an AOT^- anion on the side-chain carbon of another AOT moiety.

Such a CID fragmentation for $[AOT_5Yb_2]^+$ can be attributed to two concomitant factors: (i) a supramolecular organization in which the polar heads of two-AOT are close enough to allow a nucleophilic attack of SO_3^- of an AOT^- on an ester carbon of the other AOT^-, and (ii) an enhanced electron deficiency of the ester carbon originated from the coordination of the carbonyl oxygen of the β chain with the Yb^{3+} ion that makes it particularly susceptible to a nucleophilic attack. This is consistent with the hypothesis of Moran *et al.*[29] suggesting that the carbonyl group of the β chain is strongly chelated to the counterion.

However, another concerted mechanism involving the loss of 534 Da cannot be excluded *a priori*. This mechanism would involve (Scheme 2) an alkene elimination, with a concerted loss of AOTH. The same reasons that could afford a SN2 mechanism are also feasible for such a mechanism.

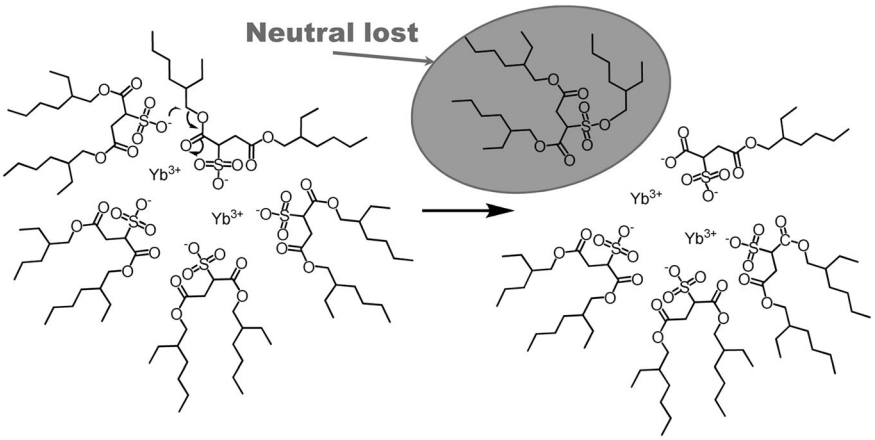

Scheme 1. Hypothetical mechanism involving intra-cluster nucleophilic attack of the SO_3^- of an AOT^- anion on the side-chain carbon of another AOT moiety.

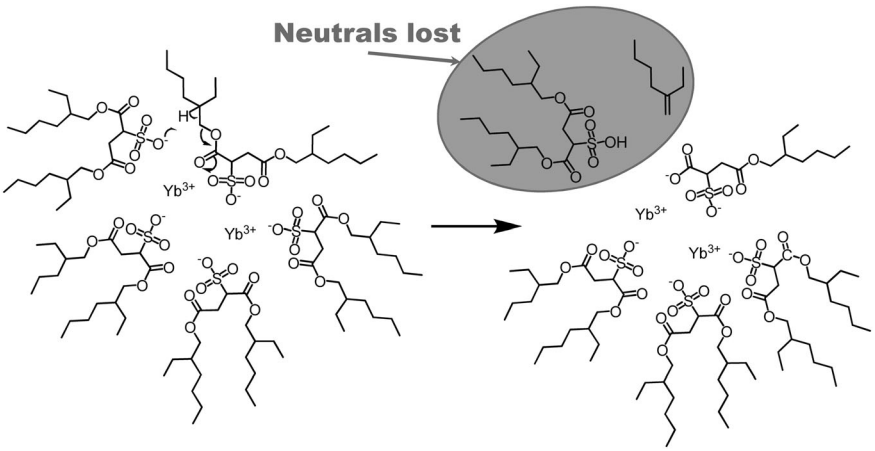

Scheme 2. Hypothetical mechanism involving alkene elimination, with a concerted loss of AOTH.

It is worth noting that a similar behavior has been observed for $[AOT_5Er_2]^+$. This confirms that charged AOT_3Yb and AOT_3Er aggregates with the same composition have the same structural arrangement and very similar chemical properties.

In order to verify the dependence of the fragmentation processes on the collision energy (CE), we performed some ER-MS experiments. By plotting the precursor ion abundance vs the CE, survival yield (SY) curves are obtained and by recording the abundances of the product ions, their yield curves (PY) are obtained. The results for $[AOT_5Ln_2]^+$ are shown in Fig. 3.

Starting from the ion $[AOT_5Yb_2–AOT–C_8H_{17}]^+$ all the further fragmentations involve consecutive losses of C_8H_{16} (112 Da). These losses are due to the fragmentation of the side chain of the AOT skeleton with H-rearrangement. The elimination of C_8H_{16} (112 Da) has been observed in CID experiments on alkali metal AOT gaseous associations arising from $[(AOT)_nMe_{(n+1)}]^+$ (Me = Li,Na,K, Rb) at high CE.[10,11] Furthermore, this is the main fragmentation route that occurs on increasing the bond strength between the SO_3^- group and the metal ion. In fact elimination of alkene is a much more abundant fragmentation process for those aggregates with divalent cations, and particularly for the AOT–Co aggregates.[25]

$[AOT_8Ln_3]^+$

As is clearly shown by the SY and PY curves, the CID processes of $[AOT_8Ln_3]^+$ are very simple. The lower energy requirement for fragmentation involves the elimination of neutral $[AOT_3Ln]$ species and the loss of AOT-C_8H_{17} (534 Da) as consecutive reaction (Supplementary Fig. S3, Supporting Information).

It is interesting to note that the loss of AOT_3Ln, that constitutes the preferred fragmentation route of $[AOT_8Ln_3]^+$, is not present for $[AOT_5Ln_2]^+$. This highlights the relative high stability of the $[AOT_5Ln_2]^+$ species.

Mixed AOT Na and Ln aggregates

$[AOT_3LnNa]^+$

The MS/MS experiments of $[AOT_3LnNa]^+$ show at low CE (lab CE 20 eV) only the loss of C_8H_{16} (112 Da). At higher collision energy, the $[AOT_3LnNa–C_8H_{16}]^+$ ion undergoes two competitive fragmentation reactions involving a further elimination of C_8H_{16} or of AOT-C_8H_{17} (534 Da) as neutral fragments (Fig. 4). It is interesting to note that in this case the loss of AOT–C_8H_{17} is not the preferred reaction at low CE, but it occurs as a consecutive reaction after the alkene elimination.

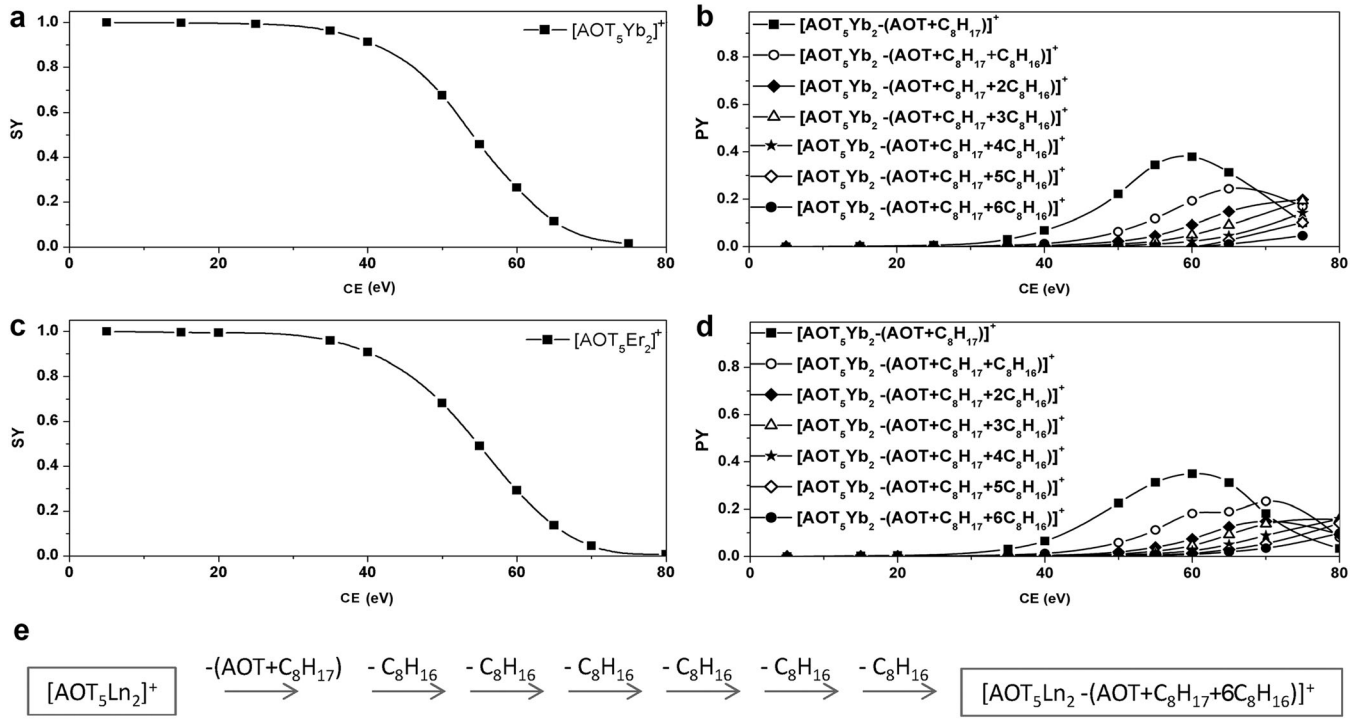

Figure 3. $[AOT_5Yb_2]^+$: (a) SY curve, (b) PY curves; $[AOT_5Er_2]^+$, (c) SY curve, (d) PY curves, and (e) schematic fragmentation pathways of $[AOT_5Ln_2]^+$.

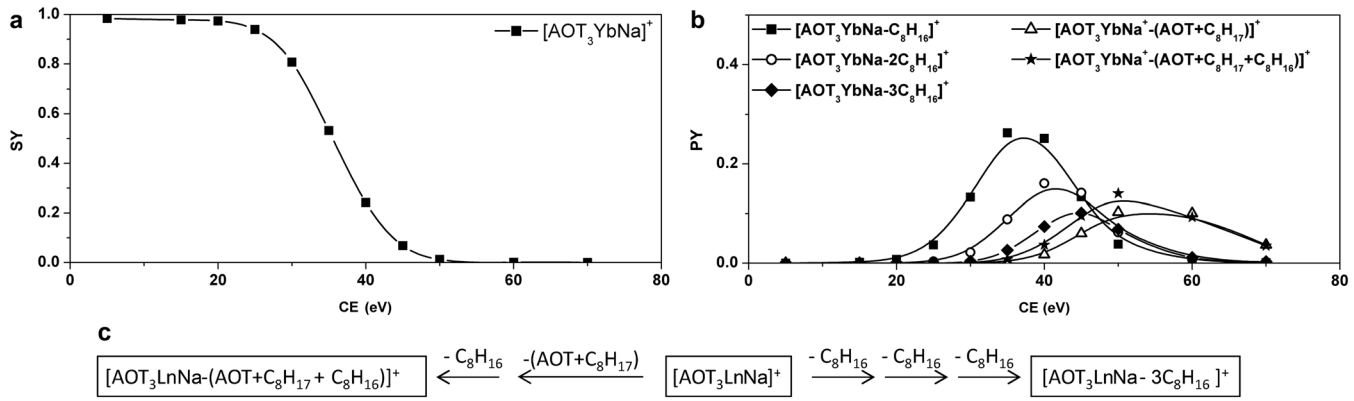

Figure 4. $[AOT_3YbNa]^+$: (a) SY curve, (b) PY curves, and (c) schematic fragmentation pathways of $[AOT_3LnNa]^+$.

$[AOT_4LnNa_2]^+$

For $[AOT_4LnNa_2]^+$ the first observed losses are those of AOTNa (444 Da) and AOT–C_8H_{17} (534 Da) with practically the same abundance. The ion formed by AOTNa elimination behaves similarly to $[AOT_3LnNa]^+$. In fact, at higher energies, it undergoes consecutive losses of C_8H_{16} (Supplementary Fig. S4, Supporting Information).

$[AOT_6Ln_2Na]^+$

In the case of $[AOT_6Ln_2Na]^+$, three competitive elimination pathways take place and are indicated as *routes 1*, *2* and *3*, respectively. *Route 1*, originated from a neutral loss of $(AOT)_3Yb$, is the most abundant. The resulting product ion is assigned to $[AOT_3YbNa]^+$ and this ion can further lose one or more C_8H_{16} molecules (112 Da, supposedly 2-ethyl-1-hexene), affording minor intensity peaks belonging to the series $[AOT_3YbNa–(k\ C_8H_{16})]^+$, with $k = 1–3$.[10,11]

Fragmentation *routes 2* and *3* are characterised by competitive neutral losses of AOTNa and AOT-C_8H_{17}, respectively (the same neutral loss as described in Scheme 1 or 2). This ion in turn undergoes consecutive C_8H_{16} elimination (Supplementary Fig. S5, Supporting Information).

Negative ion ESI-MS spectra of $(AOT)_3Yb$ and $(AOT)_3Er$

To evaluate negative ion mode behaviour, the ESI-MS spectra of $(AOT)_3Yb$ and $(AOT)_3Er$ in CH_3CN solutions were examined. In this case also the spectra of $(AOT)_3Yb$ and $(AOT)_3Er$ were recorded at 35 V and 170 V cone

voltages. The results are summarized in Fig. 5 for $(AOT)_3Yb$ and in Supplementary Fig. S6 (Supporting Information) for $(AOT)_3Er$.

The spectra show a collection of peaks consistent with clusters of AOT^- and lanthanides (Ln, Ln = Yb, Er) due to $[(AOT)_{3m+1} + mLn]^-$ species (with $1 \leq m \leq 4$), and peaks due to species characterized by the participation of environmental Na^+ ions ($[(AOT)_n + mLn + pNa]^-$ species (with $4 \leq n \leq 11$; $1 \leq m \leq 3$ and $1 \leq p < 2$). For $(AOT)_3Ln$ the ESI-MS spectra at 35 V and 170 V show the same aggregates, with the most abundant peak (except for the AOT^- peak at *m/z* 421.2) being due to the species $[AOT_4Ln]^+$, accompanied by other peaks attributable to larger aggregates containing exclusively AOT and Ln as well as aggregates containing both Ln and Na. In the case of the erbium aggregates, small peaks, due to in-source fragmentation, were observed at 35 V and 170 V cone voltages. These peaks are all due to the loss of the $C_{20}H_{37}O_4$ moiety from the corresponding aggregate at higher *m/z* values.

Negative ion ESI-MS/MS experiments on AOT_3Yb and AOT_3Er aggregates

The structure and fragmentation patterns of the negatively charged aggregates were also studied by CID. As representative of AOT-Ln associations (Ln = Yb, Er), we studied $[AOT_4Ln]^-$ and $[AOT_7Ln_2]^-$ as these were the most abundant species in negative ion mode. The same approach as that followed for positive ion mode MS/MS experiments was adopted.

CID experiments of $[AOT_4Ln]^-$ were performed by selecting the ion at *m/z* 1857 for Yb and the ion at *m/z* 1852 for Er, as precursor ions. From the lowest CE up to 45 eV both product ion spectra show only a peak at *m/z* 421 due to the AOT^- species. From 45 eV up to 60 eV a further peak at *m/z* 81 corresponding to the HSO_3^- ion appears and at 65 eV this ion reaches a maximum relative abundance of 15%.The trend clearly indicates that the HSO_3^- ion arises by decomposition of the AOT^- ion (*m/z* 421) (Fig. 6).

The $[AOT_7Ln_2]^-$ MS/MS spectra show only the peak corresponding to $[AOT_4Ln]^-$ up to 35 eV CE, while at higher energies a further peak at *m/z* 421, corresponding to AOT^-, appears, and this becomes the base peak at 81 eV (data not shown).

Stability of AOT-Ln aggregates

In order to obtain some information on the relative stability of AOT Ln monocharged aggregates we performed ER-MS experiments. It must be pointed out that the CE corresponding to the fragmentation of 50% of a precursor ion ($CE_{50\%}$) is generally used as a suitable parameter related to the stability. However, in order also to take into account the size effect,[30] it seemed more useful to use the kinetic energy in the center-of-mass, associated to a 50% survival yield of the precursor ions. This quantity is calculated according to Eqn. (1):

$$KE_{com50\%} = KElab_{50\%} * m_g / (m_g + m_i) \quad (1)$$

where m_g is the mass of the target gas and m_i the mass of the ion of interest.

The kinetic energy in the center-of-mass corresponds to the maximum energy transferred to the aggregate as internal energy in the case of an inelastic binary collision with the neutral target gas, when 50% of the precursor ion ($KE_{com50\%}$) is fragmented.[13,31] The $KE_{com50\%}$ values derived by $CE_{50\%}$ survival yields of the precursor ions, together with the main neutral species lost, are reported in Table 1.

An inspection of Table 1 shows that Yb or Er aggregates with the same composition have substantially identical $KE_{com50\%}$ values (within the experimental error, relative standard deviation (RSD) ≤10%) evidencing once more that the stabilities and the structure of the aggregates do not depend on the particular lanthanide (Yb or Er) involved. A comparison of the $KE_{com50\%}$ values of positively and negatively charged aggregates with the same or similar aggregation number suggests that the stability of positively charged aggregates is greater than that of negatively charged ones ($[AOT_4LnNa_2]^+ > [AOT_4Ln]^-$; $[AOT_8Ln_3]^+ > [AOT_7Ln_2]^-$; $[AOT_6Ln_2Na]^+ > [AOT_7Ln_2]^-$) evidencing a net charge effect similar to that observed for AOT-Na aggregates.[13]

Finally, the loss of AOT_3Ln is the most abundant process and the one that requires the lower amount of energy both for negatively charged aggregates and for $[AOT_8Ln_3]^+$ and $[AOT_6Ln_2Na]^+$. Even if theoretically possible, this loss is not present in the other positively charged species. This could be due to a structural requirement involving at least a Ln^{3+} coordinated with three AOT^- anions either in charged or neutral species.

Other interesting findings concern the behavior of the tetramer $[AOT_4LnNa_2]^+$ for which both AOT_3Ln and AOTNa could be competitively lost as neutral species. Instead, only

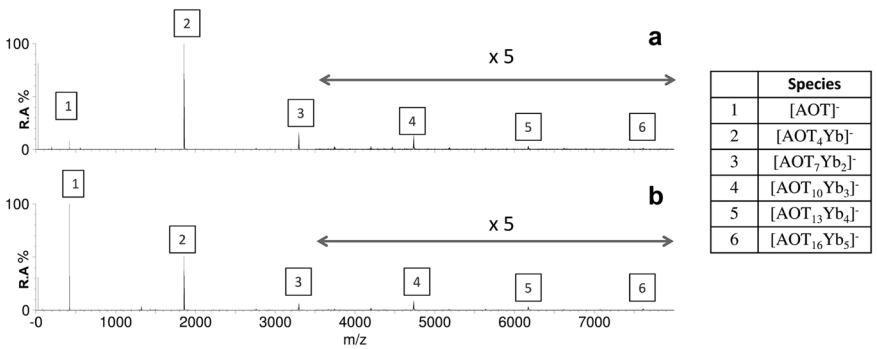

	Species
1	$[AOT]^-$
2	$[AOT_4Yb]^-$
3	$[AOT_7Yb_2]^-$
4	$[AOT_{10}Yb_3]^-$
5	$[AOT_{13}Yb_4]^-$
6	$[AOT_{16}Yb_5]^-$

Figure 5. ESI-MS spectra (negative ion mode) of AOT_3Yb at cone voltage values of (a) 35 V and (b) 170 V.

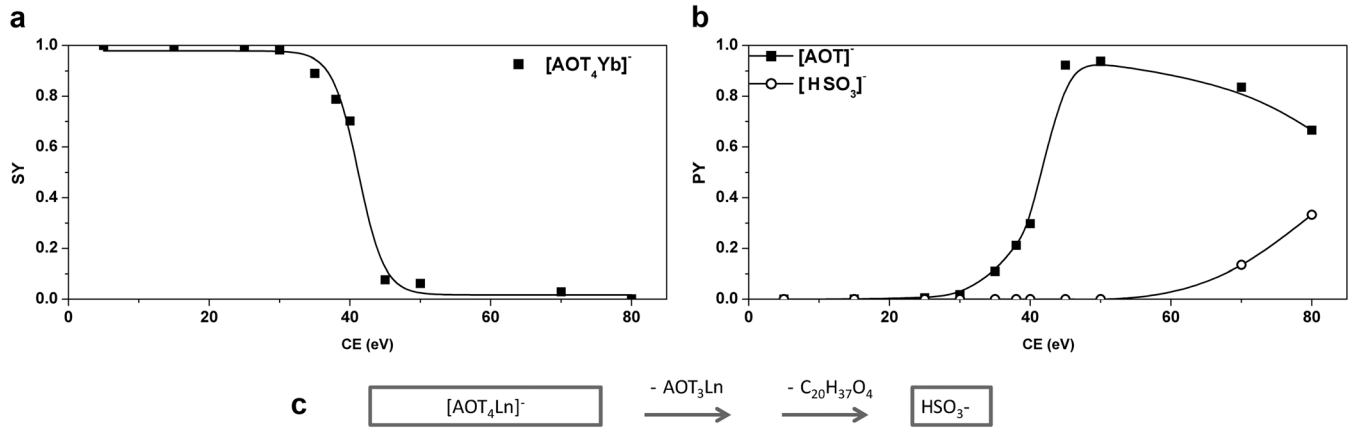

Figure 6. $[AOT_4Yb]^-$: (a) SY curve, (b) PY curves, and (c) schematic fragmentation pathways of $[AOT_4Ln]^-$.

Table 1. Positively and negatively charged AOT-Ln (Yb, Er) aggregates and their centre-of-mass kinetic energy ($KE_{com50\%}$) required to dissociate 50% of the precursor ion in CID experiments

Precursor ion	$KE_{com50\%}$ (eV)	Main neutral lost
$[AOT_5Ln_2]^+$	0.83 (Yb) 0.87 (Er)	AOT-C_8H_{17}
$[AOT_8Ln_3]^+$	0.56 (Yb) 0.54 (Er)	AOT_3Ln
$[AOT_3LnNa]^+$	0.93 (Yb) 0.93 (Er)	C_8H_{16}
$[AOT_4LnNa_2]^+$	0.97 (Yb) 0.98 (Er)	AOTNa AOT-C_8H_{17}
$[AOT_6Ln_2Na]^+$	0.74 (Yb) 0.78 (Er)	AOT_3Ln
$[AOT_4Ln]^-$	0.89 (Yb) 0.93 (Er)	AOT_3Ln
$[AOT_7Ln_2]^-$	0.50 (Yb) 0.49 (Er)	AOT_3Ln

the loss of AOTNa is observed unless the CE is very high. Indeed the abundance of $[AOTNa_2]^+$ reaches its maximum value (about 10% with respect to the $[AOT_4LnNa_2]^+$ ion) when the CE is 50 eV. From a thermodynamic point of view these competitive reactions could be related to the competition of neutral AOTNa and AOT_3Ln to link to a free Na^+. The results indicate that the sodium ion affinity for AOT_3Ln is significantly higher than that for AOTNa. Another observation is that the $KE_{com50\%}$ value for $[AOT_4LnNa_2]^+$ (0.97–0.98 eV) is very close to that for $[AOT_4Na_5]^+$ (about 1 eV) obtained with the same instrument and experimental conditions.[13] This could be read that there is an identical energy requirement to remove AOTNa from $[AOT_4Na_5]^+$ or $[AOT_4LnNa_2]^+$ that could be linked to the overcoming of similar electrostatic binding forces.

CONCLUSIONS

Detailed information on the stability and structural features of positively and negatively singly charged aggregates of AOT_3Yb and AOT_3Er in vacuum has been obtained by ESI-MS, CID experiments and energy-resolved mass spectrometry.

The ESI-MS spectra are dominated by singly charged species that show a larger aggregation number in positive ion mode. The CID experiments for the positively charged aggregates containing Ln show different behaviour depending on the species considered.

It is possible distinguish three elimination pathways: the most abundant route is the loss of a neutral fragment $(AOT)_3Yb$, which requires the lowest energy.

When this route is not possible, two competitive fragmentation pathways can be followed: a loss of one or more C_8H_{16} (112 Da) molecules, or a loss of nominal mass 534 Da, assigned to $C_{28}H_{54}O_7S$. Two alternative fragmentation mechanisms have been proposed, both consistent with an ordered supramolecular aggregation.

The negative ion MS experiments showed the importance of the $[AOT_4Ln]^-$ ion as the basic synthon for the assembly of larger aggregates. Is also evidenced that both lanthanide aggregates show upon ER-MS experiments the same stabilities, implying a similar supramolecular organization.

Acknowledgements

Research Funds of the University of Palermo are gratefully acknowledged for financial support.

REFERENCES

[1] L. Ceraulo, G. Giorgi, V. Turco Liveri, D. Bongiorno, S. Indelicato, F. Di Gaudio, S. Indelicato. Mass spectrometry of surfactant aggregates. *Eur. J. Mass Spectrom.* **2011**, *17*, 525.
[2] D. Bongiorno, L. Ceraulo, M. Ferrugia, F. Filizzola, A. Longo, A. Mele, A. Ruggirello, V. Turco Liveri. Localization and interactions of melatonin in dry cholesterol/lecithin mixed reversed micelles used as cell membrane models. *Int. J. Pharmaceut.* **2006**, *312*, 96.
[3] D. Bongiorno, L. Ceraulo, M. Ferrugia, F. Filizzola, A. Ruggirello, V. Tutrco Liveri. Localization and interactions of melatonin in dry cholesterol/lecithin mixed reversed micelles used as cell membrane models. *J. Pineal Res.* **2005**, *38*, 292.
[4] M. Sharon, L. L. Ilag, C. V. Robinson. Evidence for micellar structure in the gas phase. *J. Am. Chem. Soc.* **2007**, *129*, 8740.

[5] G. Giorgi, L. Ceraulo, V. Turco Liveri. Surfactant self-assembling in the gas phase: bis(2-ethylhexyl)sulfosuccinate divalent metal ion anionic aggregates. *Rapid Commun. Mass Spectrom.* **2012**, *26*, 2260.

[6] J. Siuzdak, B. Bothner. Gas-phase micelles. *Angew. Chem. Int. Ed.* **1995**, *34*, 2053.

[7] Y. Fang, A. Bennett, J. Liu. Multiply charged gas-phase NaAOT reverse micelles: Formation, encapsulation of glycine and collision-induced dissociation. *Int. J. Mass Spectrom.* **2010**, *293*, 12.

[8] Y. Fang, A. Bennett, J. Liu. Selective transport of amino acids into the gas phase: driving forces for amino acid solubilization in gas-phase reverse micelles. *Phys. Chem. Chem. Phys.* **2011**, *13*, 1466.

[9] G. De Petris, M. R. Festa, M. R. L. Galantini, E. Giglio, C. Leggio, N. V. Pavel, A. Troiani. Sodium glycodeoxycholate and glycocholate mixed aggregates in gas and solution phases. *J. Phys. Chem. B* **2009**, *113*, 7162.

[10] F. Cacace, G. De Petris, E. Giglio, F. Punzo, A. Troiani. Bile salt aggregates in the gas phase: an electrospray ionization mass spectrometric study. *Chem. Eur. J.* **2002**, *8*, 1925.

[11] D. Bongiorno, L. Ceraulo, A. Ruggirello, V. Turco Liveri, E. Basso, R. Seraglia, P. Traldi. Surfactant self-assembling in gas phase: electrospray ionization- and matrix-assisted laser desorption/ionization-mass spectrometry of singly charged AOT clusters. *J. Mass Spectrom.* **2005**, *40*, 1618.

[12] G. Giorgi, L. Ceraulo, V. Turco Liveri. Surfactant self-assembly in the gas phase: bis(2-ethylhexyl) sulfosuccinate-alkaline metal ion aggregates. *J. Phys. Chem. B* **2008**, *112*, 1376.

[13] D. Bongiorno, L. Ceraulo, G. Giorgi, S. Indelicato, A. Ruggirello, V. Turco Liveri. Supramolecular aggregates in vacuum: Positively mono-charged sodium alkanesulfonate clusters. *Eur. J. Mass Spectrom.* **2010**, *16*, 151.

[14] G. Longhi, S. Fornili, V. Turco Liveri, S. Abbate, D. Rebbeccani, L. Ceraulo, F. Gangemi. Sodium bis(2-ethylhexyl) sulfosuccinate self-aggregation in vacuo: molecular dynamics simulation. *Phys. Chem. Chem. Phys.* **2010**, *12*, 4694.

[15] G. Longhi, S. Abbate, L. Ceraulo, A. Ceselli, S.L. Fornili, V. Turco Liveri. A molecular dynamics study of structure, stability and fragmentation patterns of sodium bis(2-ethylhexyl)sulfosuccinate positively charged aggregates in vacuo. *Phys. Chem. Chem. Phys.* **2011**, *13*, 21423.

[16] D. Bongiorno, L. Ceraulo, G. Giorgi, S. Indelicato, M. Ferrugia, A. Ruggirello, V. Turco Liveri. Effects of the net charge on abundance and stability of supra- molecular surfactant aggregates in gas phase. *J. Mass Spectrom.* **2011**, *46*, 195.

[17] G. Giorgi, L. Ceraulo, G. Berden, J. Oomens, V. Turco Liveri. Gas phase infrared multiple photon dissociation spectra of positively charged sodium bis(2-ethylhexyl) sulfo-succinate reverse micelle-like aggregates. *J. Phys. Chem.* **2011**, *115*, 2282.

[18] S. Indelicato, D. Bongiorno, S. Indelicato, L. Drahos, V. Turco Liveri, L. Turiak, K. Vekey, L. Ceraulo. Degrees of freedom effect on fragmentation in tandem mass spectrometry of singly charged supramolecular aggregates of sodium sulfonates. *J. Mass Spectrom.* **2013**, *48*, 379.

[19] D. Bongiorno, L. Ceraulo, G. Giorgi, S. Indelicato, V. Turco Liveri. Do electrospray mass spectra of surfactants mirror their aggregation state in solution? *J. Mass. Spectrom.* **2011**, *46*, 1263.

[20] D. Bongiorno, S. Indelicato, G. Giorgi, S. Scarpella, V. Turco Liveri and L. Ceraulo. Electrospray ion mobility mass spectrometry of positively charged sodium bis(2-ethylhexyl)sulfosuccinate aggregates. *Eur. J. Mass Spectrom.* **2014**, *20*, 169.

[21] A. J. Borysik and C. V. Robinson. The 'sticky business' of cleaning gas-phase membrane proteins: a detergent oriented perspective. *Phys. Chem. Chem. Phys.* **2012**, *14*, 14439.

[22] A. J. Borysik and C. V. Robinson. Formation and dissociation processes of gas-phase detergent micelles. *Langmuir* **2012**, *28*, 7160.

[23] G. Giorgi, E. Giocaliere, L. Ceraulo, A. Ruggirello, V. Turco Liveri. Spatially ordered surfactant assemblies in the gas phase: negatively charged bis(2-ethylhexyl)sulfosuccinate-alkaline metal ion aggregates. *Rapid Commun. Mass Spectrom.* **2009**, *23*, 2206.

[24] G. Giorgi, L. Ceraulo, V. Turco Liveri. Characterization of gas phase aggregates of bis(2-ethylhexyl)sulfosuccinate (AOT) and divalent metal ions. Elimination of radical species in the decomposition pathways of even-electron $[AOTMIICl_2]^-$ anions. *J. Mass Spectrom.* **2012**, *47*, 1537.

[25] G. Giorgi, I. Pini, L. Ceraulo, V. Turco Liveri. Gas phase charged aggregates of bis-(2-ethylhexyl)sulfosuccinate (AOT) and divalent metal ions. First evidence of AOT solvated. *J. Mass Spectrom.* **2011**, *46*, 925.

[26] C. Bazzini, S. Brovelli, T. Caronna, C.Gambarotti, M. Giannone, P. Macchi, F. Meinardi, A. Mele, W. Panzeri, F. Recupero, A. Sironi, R. Tubino. Synthesis and characterization of some aza[5]helicenes. *Eur. J. Org. Chem.* **2005**, 1247.

[27] S. Abbate, C. Bazzini, T. Caronna, F. Fontana, C. Gambarotti, F. Gangemi, G. Longhi, A. Mele, I. Natali Sora, W. Panzeri. Monoaza[5]helicenes. Part 2: Synthesis, characterisation and theoretical calculations. *Tetrahedron* **2006**, *62*, 139.

[28] S. Abbate, T. Caronna, A. Longo, A. Ruggirello, V. Turco Liveri. Study of confined 5-aza[5]helicene in ytterbium(III) bis(2-ethylhexyl) sulfosuccinate reversed micelles. *J. Phys. Chem. B* **2007**, *111*, 4089.

[29] P. D. Moran, A. G. Bowmaker, R. P. Cooney, J. R. Bartlett, J. L. Woolfrey. Vibrational spectra of metal salts of bis (2-ethylhexyl)sulfosuccinate. *J. Mater. Chem.* **1995**, *5*, 295.

[30] A. Memboeuf, A. Nasioudis, S. Indelicato, F. Pollreisz, A. Kuki, S. Kéki, O. F. Van den Brink, K. Vékey, L. Drahos. Size effect on fragmentation in tandem mass spectrometry. *Anal. Chem.* **2010**, *82*, 2294.

[31] V. Gabelica, E. De Pauw. Internal energy and fragmentation of ions produced in ESI sources. *Mass Spectrom. Rev.* **2005**, *24*, 566.